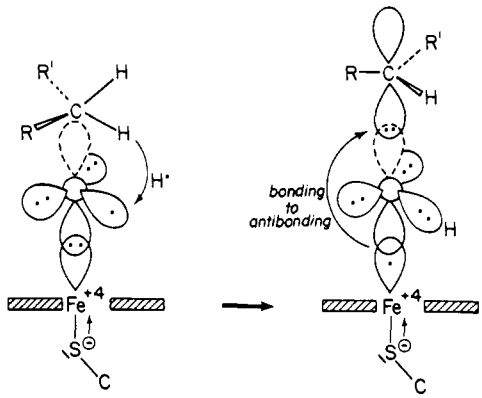

Figure 2. The product formation step in the mono-oxygenase reaction. The inversion of the oxygen orbitals is driven by a concerted stabilization of the carbon radical in the Fe–O antibonding orbital, along with a low-energy bonding to antibonding excitation.

presence of an oxy radical species within 0.7 kcal/mol of the ground state. This species is apparently stabilized as the iron–oxygen bond is lengthened.[11] In Scheme I we show the equilibrium between two isoelectronic iron–oxo structures involving thiolate ligated heme. We suggest that, since the overall complex has neutral charge and S → Fe π electron donation occupies the iron dπ orbitals (reducing the iron–oxygen bond order), the system will tend to the oxygen radical configuration **2** instead of the "compound I" like cation radical **1**. The overall neutral charge of the thiolate system ensures that, barring heme pocket polarization effects, **1** must lie at higher energy, since it corresponds to the spontaneous creation of an electric dipole in a non-polar environment. Thiolate ligated heme proteins such as chloroperoxidase,[12] which apparently utilize compound I intermediates and have a lower probability for hydroxylation reactions, must have polar heme pockets[13] that tend to stabilize the porphyrin cation radical of **1**.

Scheme II displays the analogous isoelectronic states in histidine-ligated heme proteins. Here the net charge on the complex is +1 and the positively charged "hole" is stabilized through delocalization in the π-cation radical. In addition, the absence of the thiolate π-electrons allows the Fe(dπ) orbitals to couple more effectively with the oxygen. Thus, as suggested by recent Raman[14] and EXAFS[15] data, species **3** is energetically favored in histidine-ligated complexes and the porphyrin radical is poised for electron reduction at the heme periphery[16] in the peroxidase catalytic cycle. Note, however, that the thermodynamic probability of finding the system in **4** is non-zero and formation of hydroxylated product may be possible under certain circumstances. Thus, the "branching ratio" in the chemistry of iron–oxo complexes of heme proteins may be determined by the energetics such as in Schemes I and II. Additional factors, such as substrate alignment and H_2O occupancy in the distal pocket, will also affect the product distributions.[17]

In order to be more specific about the oxo radical **2** and the hydroxylation reaction, we show in Figure 2 a sketch of the various orbitals of substrate and thiolate–iron–oxo radical. Abstraction of one[18] of the hydrogen atoms into the oxygen radical orbital would be followed by a rehybridization of the substrate carbon atom. The carbon radical can be stabilized (and oriented) by the vacant Fe–O antibonding orbital. This results in an inversion of the oxygen orbitals, analogous to the inversion of ammonia. The inversion of the orbitals is accompanied by a low-energy (Fe–O) bonding to antibonding electronic excitation that stabilizes the C–OH bond and repels the hydroxylated product away from the ferric porphyrin. It should be noted that the inversion of the oxygen orbitals will stabilize the Fe–O antibonding orbital so that the electronic excitation energy is thermodynamically favorable. It is not inconceivable that specific protein fluctuations involving the sulfur, iron, oxygen, and substrate nuclei could also help to induce the transition. Events analogous to those described above, but involving electron (rather than hydrogen atom) transfer, might also be useful in describing the epoxidation of carbon–carbon double bonds.[19]

Acknowledgment. This work was supported by NIH Grant DK 35090 and NIH Research Career Development Award DK 01405. The author is especially indebted to John Dawson and Steve Sligar for numerous stimulating discussions.

(11) Lowe, G.; Collins, J.; Luke, B.; Waleh, A.; Pudzianowski, A. *Enzyme* **1986**, *36*, 54.
(12) Bangcharoenpaurpong, O.; Champion, P. M.; Hall, K.; Hager, L. P. *Biochemistry* **1986**, *25*, 2374.
(13) Sono, M.; Dawson, J.; Hall, K.; Hager, L. *Biochemistry* **1986**, *25*, 347.
(14) Paeng, K.; Kincaid, J. *J. Am. Chem. Soc.* **1988**, *110*, 7913.
(15) Penner-Hahn, J.; Eble, K.; McMurry, T.; Renner, M.; Balch, A.; Groves, J.; Dawson, J.; Hodgson, K. *J. Am. Chem. Soc.* **1986**, *108*, 7819.
(16) Ator, M.; David, S.; Ortiz de Montellano, P. *J. Biol. Chem.* **1987**, *262*, 14954.
(17) Atkins, W.; Sligar, S. G. *J. Am. Chem. Soc.* **1987**, *109*, 3754.
(18) Gelb, M.; Heimbrook, D.; Malkonen, P.; Sligar, S. G. *Biochemistry* **1982**, *21*, 370.
(19) Traylor, T. G.; Nakano, T.; Dunlap, B. *J. Am. Chem. Soc.* **1986**, *108*, 2782.

The Methyl Group Geometry in Trichloromethyltitanium: A Reinvestigation by Gas Electron Diffraction

Peter Briant and Jennifer Green

Inorganic Chemistry Laboratory
South Parks Road, Oxford OX1 3QE, Great Britain

Arne Haaland,* Harald Møllendal, Kristin Rypdal, and Janos Tremmel

Department of Chemistry, University of Oslo
P.B. 1033, 0315 Oslo 3, Norway

Received December 8, 1988

A recent preliminary communication on the molecular structure of Cl_3TiCH_3 as determined by gas electron diffraction[1] suggested an unusual methyl group geometry: C–H bond distance 115.8 (1.6) pm and valence angle $\angle$TiCH = 101.0 (2.2)°, presumably due to partial donation of C–H bonding electrons into vacant d orbitals on Ti. Such an interaction is also consistent with the observation of an unusually large positive H,H coupling constant of +11.3 Hz and an unusually low CH_3 rocking mode of 580 cm^{-1} as compared to 825 cm^{-1} in Cl_3GeCH_3.[1]

Very recently Williamson and Hall have reported the results of extensive SCFMO and GVB calculations on Cl_3TiCH_3.[2] On the basis of structure optimizations at different levels they predict a normal C–H bond distance of 110 ± 1 pm and a slightly less-than-tetrahedral angle of 107 ± 1°.[2] The calculations reproduce the lowering of the rocking mode relative to Cl_3GeCH_3 but provide no indication for Ti··(C–H) interactions.

We prepared Cl_3TiMe (Me = CH_3 or CD_3) with the intention of determining the molecular structure by MW spectroscopy. We have, however, been unable to record a MW spectrum, probably because Cl_3TiMe decomposes rapidly on the metal walls of the waveguide. It was then decided to record the GED data for both compounds with use of an all-glass inlet system. These experiments proceeded without difficulty. We hope to record MW spectra

(1) Berry, A.; Dawoodi, Z.; Derome, A. E.; Dickinson, J. M.; Downs, A. J.; Green, J. C.; Green, M. L. H.; Hare, P. M.; Payne, M. P.; Rankin, D. W. H.; Robertson, H. E. *J. Chem. Soc., Chem. Commun.* **1986**, 520.
(2) Williamson, R. L.; Hall, M. B. *J. Am. Chem. Soc.* **1988**, *110*, 4428.
(3) For a discussion of the rocking mode of H_3TiCH_3 see also: Eisenstein, O.; Jean, Y. *J. Am. Chem. Soc.* **1985**, *107*, 1177. Shiga, A.; Kojima, J.; Sasaki, T.; Kikuzono, Y. *J. Organomet. Chem.* **1988**, *345*, 275.

0002-7863/89/1511-3434$01.50/0

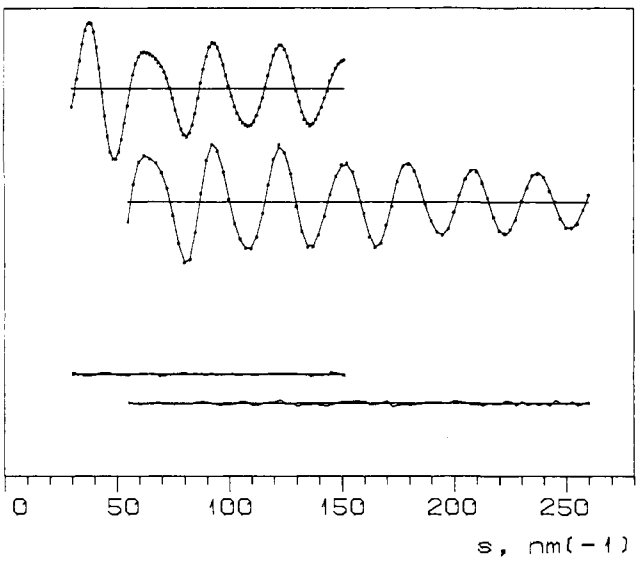

Figure 1. Experimental (●) and calculated (—) modified molecular intensity curves for Cl_3TiCH_3. Below: difference curves.

using an all-glass MW cell at Universität Tübingen and to carry out structure refinements based on both GED and MW data. In view of the great interest in metal··(C–H) interactions,[2,4,5] we wish to report the results of structure refinements on the GED data alone: these provide no indication for an unusual methyl group geometry.

Purple-black crystals of Cl_3TiMe (Me = CH_3 or CD_3) were prepared from $TiCl_4$ and $ZnMe_2$ in 2-methylbutane[1] and recrystallized twice from the same solvent. The identity of the sample was established by gas-phase IR spectra. The spectra contained a band at about 502 cm^{-1}, indicating the presence of $TiCl_4$ in the gas if not in the solid phase. (We return to this point below.) The sample was stored at −80 °C until immediately before the GED experiment. The data for Cl_3TiCH_3 were recorded with the sample at 0 °C and the inlet system at room temperature.[1] Exposures were made with nozzle-to-plate distances of 50 and 25 cm. The modified molecular intensity curves shown in Figure 1 were based on six plates for each distance. The data for Cl_3TiCD_3 were recorded with the sample at room temperature. Due to lack of material we obtained only two 50-cm plates and four 25-cm plates.

Structure refinements by least-squares calculations were based on models of C_3 symmetry. Shrinkage effects were neglected, but a thermal average dihedral angle ϕ(ClTiCH) was refined along with the three bond distances, the two valence angles, and five root-mean-square vibrational amplitudes (l). The best values are listed in Table I. The estimated standard deviations have been expanded to compensate for data correlation and a scale uncertainty of 0.1%. Calculated modified molecular intensity curves (Figure 1) and radial distribution curves (Figure 2) are in good agreement with their experimental counterparts.

The structures of Cl_3TiCH_3 and Cl_3TiD_3 are of course expected to be very similar, though the vibrational amplitude of the C–H bond is expected to be somewhat larger than that of the C–D bond: the calculated amplitudes in methane at 25 °C are l(C–H) = 7.8 pm and l(C–D) = 6.0 pm, respectively.[6] The structure parameters listed in Table I are indeed equal to well within their combined uncertainties. Bond distances and valence angles are in reasonable agreement with those obtained by Williamson and Hall by SCF calculations with their largest basis: Ti–Cl = 221.9 pm, Ti–C = 201.6 pm, C–H = 109.1 pm, ∠ClTiC = 103.7°, and ∠TiCH = 108.3°. In neither compound do we find evidence for deviations from normal methyl group geometry; deviations of the magnitude

Table I. Bond Distances (r_a), Valence Angles, and Root-Mean-Square Vibrational Amplitudes (l) of Cl_3TiMe (Me = CH_3 or CD_3) As Determined by Gas Electron Diffraction[c]

	ref 1	this work	
	Me = CH_3	Me = CH_3	Me = CD_3
Ti–Cl, pm	218.5 (3)	218.5 (3)	217.9 (3)
Ti–C, pm	204.2 (9)	204.7 (6)	204.8 (12)
C–H, pm	115.8 (16)	109.8 (6)	110.0 (9)
∠ClTiC, deg	105.2 (2)	105.6 (2)	106.0 (2)
∠TiCH, deg	101.0 (22)	109.0 (17)	108.4 (25)
ϕ,[a] deg	38	31 (5)	26 (8)
l(Ti–Cl), pm	4.4 (2)	4.6 (2)	5.0 (2)
l(Ti–C), pm	4.5 (13)	7.0 (11)	11.2 (18)
l(C–H), pm		3.9 (21)	2.0 (21)
l(Cl··Cl), pm	10.8 (11)	12.1 (6)	13.9 (15)
l(Cl··C), pm	11.7 (5)	12.4 (3)	12.9 (6)
R[b]	7.7%	2.4%	3.9%

[a] Dihedral angle ClTiCH. ϕ = 0° for eclipsed conformation. [b] $R = [\sum P(I_{exp} - I_{calc})^2/\sum PI_{exp}^2]^{1/2}$. [c] Estimated standard deviations in parentheses in units of the last digit.

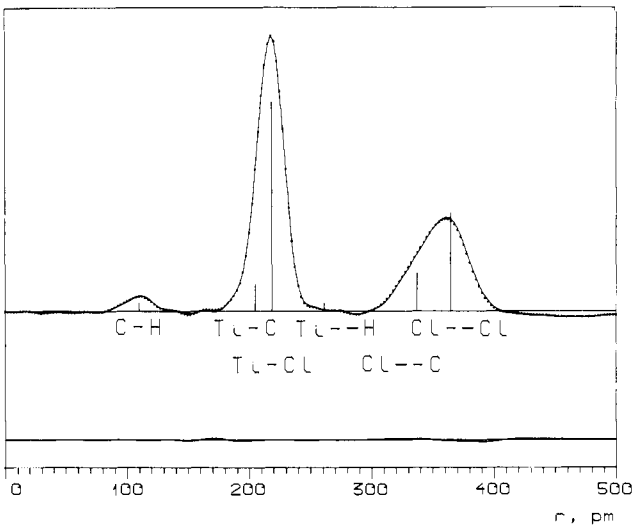

Figure 2. Experimental (●) and calculated (—) radial distribution curves for Cl_3TiCH_3. Artificial damping constant $k = 4 \times 10^{-7}$ nm^2. Below: difference curve.

suggested by Berry and co-workers appear inconsistent with our data.

In view of the reactivity and thermal instability of Cl_3TiCH_3, it appears likely that the reason for the disagreement between the GED studies is the presence of significant amounts of impurities in the molecular beam in one or both studies. We have therefore carried out additional least-squares refinements in which the mole fractions of possible $TiCl_4$[7] or methane[8] impurities were introduced as an additional parameter. Neither mole fraction refined to values significantly different from zero;[9] structure parameters and their error limits changed inconsiderably from the values listed in Table I. The presence of significant amounts of solvent molecules can be ruled out since neither the experimental RD curves nor the difference curves have a peak near 1.54 Å corresponding to C–C bond distances.

We feel that our use of an all-glass inlet system may have eliminated an important source of error. Furthermore, the flow-through nature of the experiment may have led to elimination of water and other impurities in the inlet system. Finally, we wish to point out that our studies of Cl_3TiCH_3 and Cl_3TiCD_3 represent two independent structure determinations, including the prepa-

(4) Brookhart, M.; Green, M. L. H. *J. Organomet. Chem.* **1983**, *250*, 395.
(5) Crabtree, R. H. *Chem. Rev.* **1985**, *85*, 245.
(6) Cyvin, S. J. *Molecular Vibrations and Mean Square Amplitudes*; Universitetsforlaget: Oslo, 1968; p 217f.
(7) Morino, Y.; Uehara, H. *J. Chem. Phys.* **1966**, *45*, 4543.
(8) Bartell, L. S.; Kuchitsu, K.; deNeui, R. J. *J. Chem. Phys.* **1961**, *35*, 1211.
(9) For Cl_3TiCH_3, $\chi(TiCl_4)$ = −0.01 (3) and $\chi(CH_4)$ = 0.02 (4). For Cl_3TiCD_3, $\chi(TiCl_4)$ = −0.02 (5) Å and $\chi(CD_4)$ = 0.02 (5). The numbers in parentheses are formal estimated standard deviations.

ration and purifications of the sample, and that the R factors (Table I) indicate that our experimental data are of a higher quality than those of Berry et al.

In conclusion, our study, like the calculations of Williamson and Hall, indicates that the methyl group geometry in Cl_3TiCH_3 is more or less normal; hopefully the issue will be finally resolved by a successful MW study.

Acknowledgment. We are grateful to the Norwegian Research Council for Science and the Humanities and to the VISTA program for financial support.

Stereospecific Iron Uptake Mediated by Phytosiderophore in Gramineous Plants†

Fumio Oida, Nagayo Ota, and Yoshiki Mino*

Osaka University of Pharmaceutical Sciences
Matsubara-city, Osaka 580, Japan

Kyosuke Nomoto*

Suntory Institute for Bioorganic Research
Shimamoto-cho, Mishima-gun, Osaka 618, Japan

Yukio Sugiura*

Institute for Chemical Research, Kyoto University
Uji, Kyoto 611, Japan

Received November 1, 1988

Iron is an essential element for almost all living organisms. To obtain the iron needed for proper growth, gramineous plants such as barley, wheat, and oat excrete low-molecular-weight iron chelators, generally termed phytosiderophores, from the root to solubilize and uptake iron in soil.[1] The phytosiderophores so far isolated are amino acids containing α-hydroxy carboxylate and α-amino carboxylate ligands.[2-4] In contrast, most aerobic and facultative anaerobic bacteria produce catecholate- and/or hydroxamate-type siderophores at low levels of iron(III).[5] The most typical phytosiderophore is mugineic acid (MA) (**1**),

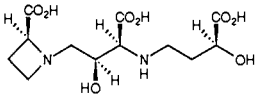

1

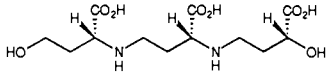

2

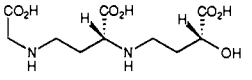

3

(2*S*,2′*S*,3′*S*,3″*S*)-*N*-[3-carboxy-3-[(3-carboxy-3-hydroxypropyl)amino]-2-hydroxypropyl]azetidine-2-carboxylic acid, excreted from the roots of barley (*Hordeum vulgare* L. var. Minorimugi). The structural, physicochemical, and biochemical properties of MA and its metal complex have been elucidated.[2,6-9]

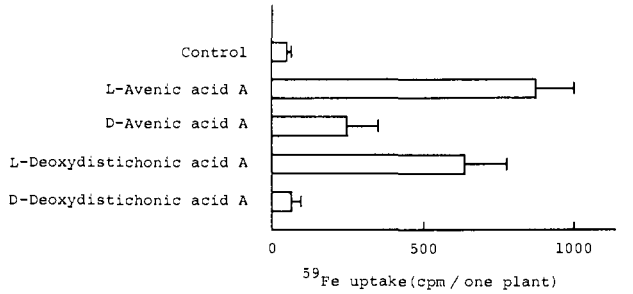

Figure 1. Effect of the optical isomers of phytosiderophore on iron-uptake in water-cultured rice plant. The experiments were performed in the same manner as reported previously.[8] The samples contained 20 μM iron (as $FeCl_3$) and 2 ppm chelator, and the control lacked only chelator from the sample.

The most salient feature among them is that the phytosiderophore facilitates not only the iron uptake but also iron utilization by the plant, whereas desferrioxamine and EDTA, which are capable of solubilizing iron as much as or more than MA, have remarkably small iron-uptake ability relative to the control.[8] This observation seems to suggest the existence of a special (stereospecific) iron-transport system in the membrane of the root.

In order to clarify this point, we synthesized the enantiomers of phytosiderophore, namely enantioavenic acid A (D-AA) (**2**) and enantiodeoxydistichonic acid A (D-DDA) (**3**), and then compared their iron-uptake ability with those of the corresponding natural phytosiderophores, L-AA[3] and L-DDA.[10] In the enantiomeric ligands, the configuration of COOH and H is a mirror relation.

D-AA and D-DDA were synthesized as follows: D-α-Hydroxy-γ-butyrolactone (**4**),[11] available from D-malic acid, was converted into a diastereomeric mixture of tetrahydropyranylated (THP) derivatives. After hydrolysis of the THP derivative, followed by benzylation, the oxidation with pyridinium chlorochromate (PCC) yielded D-malic half-aldehyde (**5**). Coupling of the half-aldehyde with the homoserine moiety (**6**) was carried out via a reductive amination procedure (sodium cyanoborohydride)[12] and resulted in the formation of the desired lactone amine (**7**). After protection of **7** with di-*tert*-butyl dicarbonate, successive treatments (2.5% KOH, $PhCH_2Br$; see Scheme I) produced the dibenzyl ester. In the same manner (oxidation with PCC), the corresponding aldehyde (**8**) was derived. This compound is an important intermediate for the syntheses of MA derivatives because the coupling with one homoserine moiety or glycine, followed by the removal of the protecting groups and hydrolysis with alkali (KOH), gave D-AA or D-DDA, respectively. Finally, treatment with Dowex 50W (H^+ form), elution with 2 N ammonia, and subsequent Sephadex G-10 chromatography yielded optically pure D-AA ($[\alpha]_D$ -16.5°, 2 N HCl, *c* 0.1) or D-DDA ($[\alpha]_D$ +8.95°, H_2O, *c* 0.1). A full report will be published elsewhere.[13]

L-AA was synthesized by the method of Ohfune et al.,[14] and L-DDA was obtained by using glycine instead of L-homoserine in the final coupling step.

These synthetic compounds were identified by mass, ^1H NMR, and ^{13}C NMR spectra. Each D form gave essentially the same spectral data as the corresponding L form. In addition, the optical rotation ($[\alpha]_D$) showed the same absolute value (16.5°, 2 N HCl, *c* 0.1 for L-AA; -8.95°, H_2O, *c* 0.1 for L-DDA) but opposite sign,

† This paper is dedicated to Prof. Haruaki Yajima on the occasion of his retirement from Kyoto University in March 1989.

(1) Sugiura, Y.; Nomoto, K. *Struct. Bonding (Berlin)* **1984**, *58*, 25-87.
(2) Takemoto, T.; Nomoto, K.; Fushiya, S.; Ouchi, R.; Kusano, G.; Hikino, H.; Takagi, S.; Matsuura, Y.; Kakudo, M. *Proc. Jpn. Acad.* **1978**, *54*, 469-473.
(3) Fushiya, S.; Sato, Y.; Nozoe, S.; Nomoto, K.; Takemoto, T. *Tetrahedron Lett.* **1980**, 3071-3072.
(4) Nomoto, K.; Yoshioka, H.; Arima, M.; Fushiya, S.; Takagi, S.; Takemoto, T. *Chimia* **1981**, *35*, 249-250.
(5) Hider, R. C. *Struct. Bonding (Berlin)* **1984**, *58*, 25-87.
(6) Mino, Y.; Ishida, T.; Ota, N.; Inoue, M.; Nomoto, K.; Yoshioka, H.; Takemoto, T.; Sugiura, Y.; Tanaka, H. *Inorg. Chem.* **1981**, *20*, 3440-3444.
(7) Sugiura, Y.; Tanaka, H.; Mino, Y.; Ishida, T.; ota, N.; Inoue, M.; Nomoto, K.; Yoshioka, H.; Takemoto, T. *J. Am. Chem. Soc.* **1981**, *103*, 6979-6982.
(8) Mino, Y.; Ishida, T.; ota, N.; Inoue, M.; Nomoto, K.; Takemoto, T.; Tanaka, H.; Sugiura, Y. *J. Am. Chem. Soc.* **1983**, *105*, 4671-4676.
(9) Iwashita, T.; Mino, Y.; Naoki, H.; Sugiura, Y.; Nomoto, K. *Biochemistry* **1983**, *22*, 4842-4845.

(10) L-DDA has not been isolated yet as a natural product, whereas distichonic acid (L-DA) is a phytosiderophore excreted from the roots of beer barley (*Hordeum vulgare* L. distichum). L-DDA is thought to have an ability similar to that of the natural phytosiderophores, however, because the artificial phytosiderophore contains the six functional groups that participate in the complexation with metal ions such as Fe(III) and Co(III).

(11) Collum, D. B.; McDonald, J. H., III; Still, W. C. *J. Am. Chem. Soc.* **1980**, *102*, 2117-2118.
(12) Borch, R. F.; Bernstein, M. D.; Dust, H. D. *J. Am. Chem. Soc.* **1971**, *93*, 2897-2904.
(13) Ohfune, Y., et al., manuscript in preparation.
(14) Ohfune, Y.; Nomoto, K. *Chem. Lett.* **1981**, 827-828.

0002-7863/89/1511-3436$01.50/0